Received: 21 November 2021 | Revised: 18 July 2022 | Accepted: 7 November 2022

DOI: 10.1002/hyp.14761

SPECIAL ISSUE PAPER

WILEY

Forest stand complexity controls ecosystem-scale evapotranspiration dynamics: Implications for landscape flux simulations

Rhoswen Leonard[1] | Paul Moore[2] | Stefan Krause[1] | Laura Chasmer[3] | Kevin J. Devito[4] | Richard M. Petrone[5] | Carl Mendoza[6] | James Michael Waddington[2] | Nicholas Kettridge[1]

[1]School of Geography, Earth and Environmental Sciences, University of Birmingham, Birmingham, UK

[2]School of Earth, Environment & Society, McMaster University, Hamilton, Ontario, Canada

[3]Department of Geography and Environment, University of Lethbridge, Lethbridge, Alberta, Canada

[4]Department of Biological Sciences, University of Alberta, Edmonton, Alberta, Canada

[5]Department of Geography and Environmental Management, University of Waterloo, Waterloo, Ontario, Canada

[6]Department of Earth and Atmospheric Sciences, University of Alberta, Edmonton, Alberta, Canada

Correspondence
Rhoswen Leonard, School of Geography, Earth and Environmental Sciences, University of Birmingham, Edgbaston, Birmingham B15 2TT, UK.
Email: rml343@alumni.bham.ac.uk

Funding information
Natural Environment Research Council studentship funding, Grant/Award Number: NE/L501712/1; Syncrude Canada Ltd.; Canadian Natural Resources Ltd., Grant/Award Number: SCL4600100599; Natural Sciences and Engineering Research Council of Canada (NSERC) Collaborative Research and Development (CRD), Grant/Award Number: CRDPJ477235-14

Abstract

Open-canopy forested systems are found across a range of terrestrial biomes. Forest structure and organization in open-canopy systems exhibit substantial controls on system process dynamics such as evapotranspiration (ET). The energy reaching sub-canopy forest layers is greater in open-canopy systems compared to closed canopy systems, with high spatiotemporal variability in the distribution of energy that both drives ET and controls sub canopy species composition and organization. Yet the impact of their structural complexity and organization on whole system ET dynamics is poorly understood. Using the BETA+ model and measured eddy covariance-based ET fluxes from a boreal treed peatland, we critically evaluate how stand compositional and organizational complexity influences ET dynamics. Model simulations iteratively increase complexity from a simple 'big-leaf' model to a model representing spatial complexity of all system layers, demonstrating the effect of each complex system component on stand ET dynamics. We show that including forest stand complexity and associated canopy and radiation variability increases ET model estimates by ~26%. In addition to changes in the ET estimates, the inclusion of this spatial complexity is shown to induce temporal variations in the simulated ET that improves model performance by reducing unexplained variance between modelled and measured ET by 10% and reducing hysteresis in model results. These results have clear implications for flux modelling of forest systems and for larger scale climate models where open canopy systems such as this dominate the landscape. Demonstrating that whilst big leaf simulation can approximate ET fluxes, the inclusion of forest-stand complexity and its influence on spatiotemporal radiation fluxes and ecohydrological processes are necessary to effectively represent ET dynamics within open canopies.

KEYWORDS
boreal forest, eddy covariance, evapotranspiration, modelling, peatland

1 | INTRODUCTION

Globally, forests occupy ~30% of the land surface (Bonan, 2008) and exhibit strong controls over the hydrological cycle (Ellison et al., 2017). Forest evapotranspiration (ET) is an important process responsible for re-distributing water both locally and globally (by re-charging atmospheric moisture) whilst, simultaneously, acting as an important water loss mechanism that controls the hydrological balance and system functioning of forests (Jackson et al., 2001). Accurate quantification and prediction of forest ET and its components is crucial to improve the understanding of hydrological, climatic, and ecosystem processes, benefiting water resource management (Brutsaert, 2010; McNaughton & Jarvis, 1983), hydrological modelling (Zhao et al., 2013), weather forecasts, and forest vulnerability to fire (Boer et al., 2016), especially under a changing climate (Brümmer et al., 2012; Helbig et al., 2020).

Vascular plants primarily control atmospheric exchange processes in dense, closed canopy systems (Black et al., 1996; Ferretti et al., 2003; Hossein et al., 1994; Leuning et al., 1994; Wallace et al., 1993; Williams et al., 2004; Wilson et al., 2001). However, many forests have open canopies with lower stem densities, often due to limiting factors such as nutrient availability and the hydrological regime. As a result, a large proportion of the available energy reaches the sub-canopy layers (Baldocchi et al., 2000) and ecosystem ET is dominated by energy exchange within the under-story (Allen, 1990; Baldocchi et al., 2000; Villegas et al., 2010; Villegas et al., 2014; Vogel & Baldocchi, 1996; Yunusa et al., 1997). Sparse canopies of this type thus have complex ET dynamics that are controlled both by the structure and complexity of each layer from the canopy top through to the soil profile beneath and the interactions of these layers (Villegas et al., 2010; Villegas et al., 2014). Plants act as roughness elements and influence airflow, turbulence regimes, mass, and energy exchange through the subcanopy (Breshears et al., 2009; Martens et al., 2000). Canopy attributes such as height, extent of leaf coverage along the stem, tree density, and leaf density and clumping also modify spatio-temporal patterns in the drivers (Green et al., 1984; Kettridge et al., 2013; Villegas et al., 2010) and controllers of ET. Canopy components not only modify the environment directly beneath them but also the environment in adjacent areas and are important in open canopies with strong spatial contrasts in canopy composition. Notably, shading reduces energy inputs directly below the canopy as well as within canopy gaps (Villegas et al., 2014).

The physical effects of forest architecture also influence species composition and organization of lower layers through processes of competition, extinction and establishment. Open-canopy systems show relatively high sub-canopy diversity because of the increased variability in environmental conditions found in sub-canopy layers (Sagar et al., 2008). This variability in sub-canopy species is an important influence on ET dynamics because different plant species (within and between functional groups) have different albedos and show significant differences in their ability to conduct water to the atmosphere (Heijmans et al., 2004a, 2004b; Lafleur, 1990; Sena et al., 2007). Evapotranspiration from the under-storey layers is therefore highly variable in space and time due to the complicated eco-hydrological system organization. This highly variable nature of ET in open canopy systems illustrates that vertical and/or horizontal aggregation of complex non-linear systems to 'big-leaf' behaviours (common within empirical models; Shuttleworth, 2007) may be inappropriate for representing stand level ET dynamics (Friend, 2001; Villegas et al., 2010; Villegas et al., 2014).

Using a boreal peatland forest as an exemplar ecosystem, this paper assesses how stand structure and compositional organization influence ET. Characteristically open-canopy, treed peatlands occupy ~24% of the boreal forest region (Joosten & Clarke, 2002), which itself makes up ~33% of global forest cover (~10% of the earth's vegetated surface; McGuire et al., 1995). Boreal peatlands are one of the world's largest terrestrial carbon stores, accounting for a conservative estimate of ~500 GtC (Bradshaw & Warkentin, 2015; Yu, 2012), which is ~60% of the global atmospheric carbon pool (~830 GtC) (Ciais et al., 2013; Joos et al., 2013; Prather et al., 2012) and about equal to all of the carbon in living terrestrial vegetation (450 to 650 GtC; Ciais et al., 2013; Prentice & Harrison, 2009). Boreal peatland forests further perform key hydrological functions at the landscape scale (Devito et al., 2005; Holden, 2005), for example by acting as important landscape water sources through the sub-humid climate of the boreal plain (Devito et al., 2017). Forested peatlands and their vital system service provisions are also subject to regular and increasing disturbances such as fire (Chapin et al., 2000); with almost 1500 km^2 affected annually, releasing 6300 Gg C $year^{-1}$ in western Canada alone (Turetsky et al., 2002). Despite their hydrological and biogeochemical importance, and exposure to increasing disturbance, boreal forest regions remain under-represented in the ET literature (Fatichi & Pappas, 2017; Watras, 2017; Zhang et al., 2009), especially boreal wetlands (Chapin et al., 2000). Advances have been made to incorporate increasing levels of heterogeneity in models of Boreal peatland ET (Kettridge et al., 2013; Sutherland et al., 2014; Sutherland et al., 2017); however, to our knowledge, assessment of how small-scale stand complexity, composition and layer inter-dependencies affect ET dynamics remains largely unknown and un-explored.

Using Boreal peat forests to assess how stand structure and related organizational complexity influence ET (informing understanding of open canopy forest ET more generally) also has clear advantages over other such systems. Boreal forests have some of the simplest structural architecture of any forest biome (Landsberg & Gower, 1997), comprised of even-aged communities as a result of frequent stand-replacing disturbances such as wildfires, insect outbreaks, and felling (Kurz & Apps, 1993; McCarthy, 2001). This relatively simple structure, combined with their relatively low taxonomic diversity (Burton, 2013) means more concentrated efforts can be applied to defining the species-specific characteristics, responses and behaviours, thus providing advantages to modelling, computing capacity and confidence in interpretation. In addition, local scale (10 m) heterogeneity is relatively even at the 100–1000 m scale across a flat open landscape (Figure 1). This reduces the impact of potentially confounding factors that would add uncertainty to direct ET measurements, which are possible at this scale using Eddy Covariance methods.

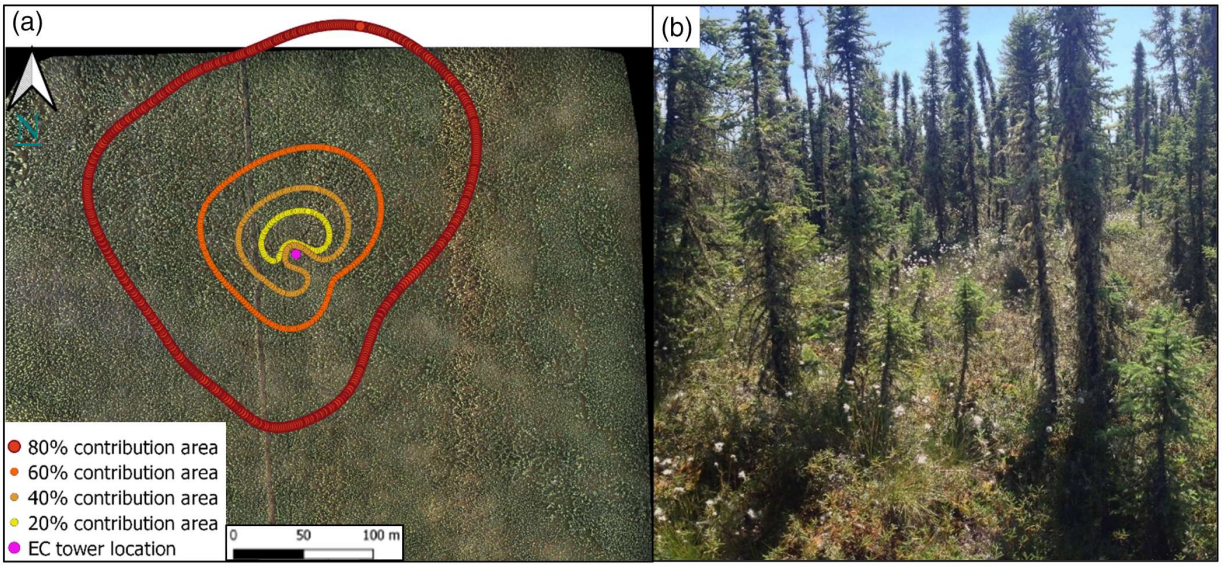

FIGURE 1 (a) Aerial image of study site showing the location of the Eddy Covariance flux tower, and the areas contributing to 20%, 40%, 60% and 80% of the total flux measured (calculated in accordance with Kljun et al. (2015) between 24th of July to 13th of August 2014 and (b) a photo of the vegetation structure.

Factors that can cause uncertainty to these direct measurements include high variability in within stand tree density/size and topographical influences. This reduction of potentially confounding factors in this context will increase confidence in model outputs and interpretation that relate directly to stand complexity effects.

This paper critically evaluates how stand compositional and organizational complexity influences ET dynamics by using an adaptation of the Boreal Ecohydrological Tree Algorithm (BETA+; Leonard et al., 2021), comparing sub-hourly ET simulations against eddy covariance (EC) flux tower measurements. Understanding how ET dynamics change by representing various system complexities within the modelling domain will provide advanced understanding of how ET is controlled by the system structure and facilitate more informed and targeted future research efforts in open-canopy forested systems.

2 | DATA AND METHODS

2.1 | Study site

Data was collected from a deep peat (≥3 m), poor fen in central Alberta (55.81° N, 115.11° W), Figure 1. The climate in this region is sub-humid with an annual mean air temperature of 1.2°C and mean annual precipitation of 483 mm (Devito et al., 2016). The surface is characterized by a ground cover mosaic, consisting of *Sphagnum. fuscum* (43% cover), *Pleurozium schreberi* (9% cover), *Cladina* and *Cladonia sp*. (11% cover) and bare peat (26% cover). The lower vascular layer comprises *Rhododendron groenlandicum*, *Rubus chamaemorus*, *Chamaedaphne calyculata*, *Maianthemum trifolia*, *Vaccinium oxycoccus*, *Vaccinium vitus-idea* and *Eriophorum sp*. The upper vascular layer comprises solely of *Picea mariana* with a stand density of 16 000 stems ha^{-1}, basal area and average height of 11 m^2 ha^{-1} and 2.3 m, respectively (Kettridge et al., 2012). Surface micro-topography varies in height by up to 0.41 m (Leonard et al., 2018).

2.2 | BETA+ model summary

BETA+ simulates ET from a treed boreal peatland (Leonard et al., 2021). Within BETA+ the landscape is discretized into discrete vertical soil profiles, with defined and differing moss and sub canopy vegetation covers (shrubs/graminoids), interspersed among a forest of trees that are individually defined in terms of location and size. Thus BETA+ uniquely accounts for small scale complexity when simulating the surface energy balance, ground-layer cover type and peat thermal behaviour and builds on previous modelling work, principally, BETA (Kettridge et al., 2013), 3-D HIP (Kettridge & Baird, 2010) and a radiative transfer model (Essery et al., 2008). Tree heights and locations are generated by a canopy height model (CHM) derived from airborne LiDAR collected at the study site (See further description in S1). The surface resistance of ground cover types was measured at the study site from *S. fuscum* ($n = 32$), *P. schreberi* ($n = 43$), *Cladina sp* ($n = 21$) and bare ground ($n = 33$). The distribution of these groundcover types (and their respective resistance [SI-1] and albedo values [SI-1]) is determined by Multivariate Adaptive Regression Splines (MARS) in accordance with Elith and Leathwick (2007) (See SI-1). Stomatal resistance and leaf area of sub-canopy vascular vegetation is randomly selected from a distribution derived from data measured at the study site (stomatal resistance and leaf area measurements were taken from *Rhododendron groenlandicum*, *Rubus chamaemorus*, *Chamaedaphne calyculata*, *Maianthemum trifolia*, and *Vaccinium vitus-idea* at the study site [SI-1]).

Meteorological data from a 10 m high tower (net radiation, upwelling shortwave radiation, air temperature, relative humidity and wind speed data) drive the surface boundary of BETA+ within which net short and longwave radiation, latent heat and sensible heat fluxes were calculated. Radiation fluxes are determined using a spatially explicit 3D radiation model that depends on tree size/position and ground cover species distribution. Trees were represented within the simulated 3D landscape as crowns (SI-1), following an approach similar to Essery et al. (2008) and adapted by Kettridge et al. (2013), which is used to determine the direct and diffuse shortwave radiation (through time) and a sky view factor (constant in time) at the sub-canopy/ground surface. Net longwave radiation is calculated from Stefan-Boltzmann law, Beer's law (Aber and Melillo, 2001) and the above generated sky view factor. The model accounts for the influence of micro-topography on the short and long wave radiation by incorporating variations in elevation, slope, aspect and shading of the peat surface (surface topography of points randomly selected from measured distributions [SI-1, Leonard et al., 2021; Kettridge & Baird, 2010]). Newton's law of cooling was used to calculate sensible heat flux. Evapotranspiration (kg m^{-2} s^{-1}) was calculated using a form of the Penman-Monteith model (Oke, 1987):

$$ET = \frac{s(T_s - T_a) + vdd_a}{r_a + r_s} \quad (1)$$

where s is the slope of the saturation vapour versus temperature curve (kg m^{-3} K^{-1}), T_s is surface temperature and T_a is air temperature (K), vdd_a is vapour density deficit of air (kg m^{-3}), r_a and r_s are aerodynamic and surface resistance (s m^{-1}), respectively. Surface resistance (r_s) is derived from field measurements of both groundcover surface resistance ($r_{GroundSurface}$) and sub-canopy stomatal resistance ($r_{vascular}$) (SI-1, Leonard et al., 2021). Tree transpiration is modelled based on measured vapour pressure deficit (cf. Thompson et al., 2014) using a transpiration efficiency derived from sap flow measurements of 15 instrumented trees at the study site (SI-1).

The 1D thermal behaviour of isolated peat profiles are simulated by a finite difference Fourier based model, discretised at 0.01 m intervals (SI-1). Bulk peat density and volumetric water content (VWC) are used to calculate the thermal properties at each node. The Van Genuchten equation is used to determine the VWC, with pore water retention determined from depth to water table with assumed hydrostatic equilibrium through the peat profile. The volumetric heat capacity of the soil profile is the sum of each soil constituent multiplied by their respective heat capacities. The latent heat of fusion is represented by increasing the volumetric heat capacity at 0°C (cf. McKenzie et al., 2007). Peat thermal conductivity is calculated in accordance with Farouki (1986), evaluated for peatlands by Kettridge & Baird (2007). Depth to water table and peat temperature were measured throughout the simulation period and used to define the water table position and the lower boundary temperature of the simulated peat profiles. When micro-topography (methods and data available in SI-1) is represented in a spatially explicit manner within BETA+, the water level remains spatially uniform, but the water table depth varies spatially as a consequence of the defined distribution in surface elevation. Microtopography data were generated from a measured distribution, derived from a Digital Elevation Model, created from a 3D point cloud generated using a structure-from-motion approach (Brown & Lowe, 2005, Moore et al., 2019). The 3D point cloud data were collected from a 10 × 10 m^2 plot at study site (more details available in SI-1). When surface micro-topography is excluded from the model, the water table depth is uniform in space, with the peat surface elevation assumed equal to the mean surface elevation (Leonard et al., 2018). Initial surface temperatures were assumed equal to air temperatures (simulations initiated at midnight). A polynomial was fit to the surface (air) and measured peat subsurface temperatures within a single temperature profile within the study site to define the initial subsurface temperatures. A detailed description of the model is available in SI-1 and Leonard et al. (2021).

2.3 | Eddy covariance

Eddy covariance data were collected using an Open Path EC system (LI7500, (LICOR), open path Infra-Red Gas Analyser (IRGA) and CSAT 3D (Campbell Scientific) sonic anemometer) from a 10 m tower between 24th July and 13th August 2014. Raw eddy covariance measurements were sampled at a frequency of 10 Hz, fluxes calculated over half-hour intervals, and saved on a CR1000 datalogger (Campbell Scientific). Net radiation (Q*) was measured using a NR-Lite net radiometer (Kipp Zonan) and a HFT3-L heat flux transducer (Campbell Scientific) was used to measure ground heat flux (Q_g). All fluxes were corrected for density, time lag and coordinate rotation (double coordinate rotation was used) following common Fluxnet protocols (Aubinet et al., 2012; Burba et al., 2012; Foken & Leclerc, 2004; Kaimal & Finningan, 1994; Leuning & Judd, 1996; Webb et al., 1980) whilst the sensors were installed level and <0.1 m apart (verified by Blanford and Gay analysis; [Blanford & Gay, 1992]) to avoid the need to account for sensor separation. The resulting half-hour fluxes were then filtered to ensure that each half-hour had at least 80% of the high-frequency records and that there was no potential for dew formation on IRGA lenses by either precipitation or by comparing the dew point temperature to the air temperature. Additional filtering removed physically improbable values and values where the difference between neighbouring fluxes were greater than ±2 standard deviations of the population. The Schuepp et al. (1990) footprint analysis was used to constrain the measured fluxes to be within 80% of the desired site boundaries. Thereafter, fluxes with a corresponding friction velocity (u^*) < 0.15 m s^{-1} were removed from the dataset. The average half-hourly energy balance closure was calculated as the ratio of the total turbulent fluxes ($Q_h + Q_e$) to available energy ($Q^* - Q_g$) and was calculated as 0.84 (with a range of −0.86–1.69). Following this the energy fluxes were forced closed, with the additional energy partitioned based on the Bowen ratio (ß) (Wilson, 2002). ß is the ratio of sensible heat (Q_h) to latent heat (Q_e). For each available half-hour, Q_e was gap-filled by scaling potential evapotranspiration (PET) (Priestley & Taylor, 1972) to ET. The scaler (α) was calculated

from the ratio between measured ET and PET for the measurement period. The average α value was 0.67.

Potential evapotranspiration (PET) was calculated according to Priestley and Taylor (1972):

$$PET = \frac{\Delta(R_n - G)}{\lambda(\Delta + \gamma)} \quad (2)$$

where PET is potential evapotranspiration (mm d^{-1}), λ is latent heat of vaporization (2.45 MJ kg^{-1}), Δ is the slope of the vapour pressure–temperature curve (kPa $°C^{-1}$), R_n is net radiation (MJ m^{-2}, per 30 min), G is soil heat flux (MJ m^{-2}, per 30 min), and γ is the psychrometric constant (kPa $°C^{-1}$).

2.4 | Description of simulations

The modelling domain was parameterised with spatially explicit data for a 250 m radius region surrounding the EC tower (80% of the total flux is contributed from within 250 m of the measurement tower 90% of the time; Figure 1a). Within the 250 m radius, ~12 000 1 m^2 simulation locations were randomly defined. For each 30-min time interval, the 2D flux footprint, calculated in accordance with Kljun et al. (2015), was used to select and weight the contributions from the given simulation points to the EC tower at 30-minute intervals for the time-period 24/07/2014 00:00 to 13/08/2014 23:30 MST (please refer to model description in section 2.2 and SI-1 for further details of how the modelling domain represents the systems vegetation structure and associated attributes). A total of 11 scenarios were simulated (Table 1), each simulation represents increasing levels of observed system complexity. The model was initially run as a simple 'big-leaf' (Single Groundcover 'Big Leaf': SGBL) with no representation of spatial variation within the vertical system layers and a single, uniform groundcover-type of either bare ground (BG), *P. scherberi* (PS), *S. fucsum* (SF), or *Cladina sp.* (C). These simulations are referred to as SGBL-BG, SGBL-PS, SGBL-SF and SGBL-C. This simulation was then repeated but with the modelling parameters associated with groundcover type (surface resistance (SI-1), and albedo) weighted by the observed relative proportions of each groundcover type (weighted ground cover big leaf; WGBL).

The next simulation in the series of increasing complexity (Weighted Groundcover, Big Leaf-Flux Foot Print: WGBL-FFP), is the same as WGBL but the radiation and canopy openness data is the mean value for each footprint area per time interval, rather than the mean value for a 250 m radius of the tower. WGSC (weighted ground cover spatially explicit canopy) is the same as the WBGL-FFP simulation but instead of having uniform radiation inputs at the ground surface, individual trees are explicitly defined, and the radiation inputs reaching the ground surface vary accordingly in space and time at each simulation point. The SGSC (spatially distributed groundcover, & spatially explicit canopy) simulation then uses the spatially distributed canopy and incoming radiation parameters to predict the spatial distribution of each groundcover type using the MARS sub-model (SI-1). The SGSCSM (spatially distributed groundcover, micro-topography & canopy) simulation further adds micro-topography influences, representing variability in slope and elevation (and water table depth) by randomly drawing from a measured distribution. The next SE (spatially explicit) simulation again builds on the previous simulation (SGSCSM) by adding spatial variability in the leaf area index (LAI) of dominant sub-canopy vascular species and surface resistance values (of both the simulated groundcover species and vascular plants) by randomly selecting values from measured distributions. Within this model, all aspects of the simulation are considered in a spatially explicit manner. The model representing most complexity, STE (Spatio-temporally Explicit) again builds on the previous simulation (SE) and adds temporal variation in surface resistance values of the groundcover species by applying an observed time relationship to the surface resistance drawn from the measured distribution (SI-1). Mann–Whitney U Tests were used to compare the measured ET data (from the EC flux data) and ET data from each BETA+ model simulation.

3 | RESULTS

3.1 | Comparison of simulated and measured data

All model simulations differed significantly from measured ET ($p < 0.05$) (Table 2). Mean measured ET for gap-filled data was 2.43 mm d^{-1} (± 3.71 SD). The big leaf scenario with a uniform cover of *Cladina spp.* (SGBL-C) showed the lowest simulated ET, underestimating measured ET by 10.68%. ET estimates were higher in SGBL-PS and SGBL-BP scenarios. A noticeably higher mean ET, was observed in SGBL-SF compared to SGBL-BP/C/PS of 1.02, 1.36 and 1.22 mm d^{-1}, respectively. When the groundcover surface resistance (r_s) and albedo was weighted to account for species composition (WGBL) the mean simulated ET was 3.15 mm d^{-1} (Table 2 and Figure 3). The simulated mean ET rose slightly by 0.48 mm d^{-1} when the mean radiation input for each time interval was used (WGBL-FFP) as opposed to the mean for the 250 m radius (80% contribution area of entire simulation period). When spatially explicit canopy and radiation inputs were added (WGSC), mean simulated ET showed a large increase, rising by 0.91 mm d^{-1}. A slight increase in mean simulated ET was observed when the MARS sub-model was added (predicting ground cover distribution, SGSC), increasing average ET by 0.13 mm d^{-1}. Minimal increase (<0.1 mm d^{-1}) was observed in mean simulated ET when micro-topography was included (SGSCSM). Mean simulated ET reduced by 0.74 mm d^{-1} in the SE simulation (Figure 3 and Table 2) when LAI of sub-canopy vascular species and the surface resistance of both groundcover and sub-canopy vascular layer were randomly drawn from measured distributions. Once temporally variable surface resistance was included (STE), the mean daily ET increased slightly by 0.08 mm d^{-1} (Table 2, Figure 3).

TABLE 1 Combinations of a uniform or spatially explicit parameterisation of forest layers for each simulated scenario.

		SGBL-PS (*P. schreberi -big-leaf*)	SGBL-SF (*S. fuscum big-leaf*)	SGBL-C (*Cladonia sp. big-leaf*)	SGBL-BP (*bare peat big-leaf*)	WGBL (*weighted groundcover big-leaf*)	WGBL FFP (*weighted groundcover & mean canopy of footprint area*)	WGSC (*weighted groundcover & spatially explicit canopy*)	SGSC (*spatially distributed groundcover, & spatially explicit canopy*)	SGSCSM (*spatially distributed groundcover, micro-topography & canopy*)	SE (*everything is spatially explicit*)	STE (*everything is spatially explicit plus time relationship of r_s*)
Radiation and canopy openness	Uniform (Mean value within 250 m radius of the flux measurement tower)	✓	☐	☐	☐	☐						
	Mean value (within the footprint at each time interval)						☐					
	Spatially explicit							☐	☐	☐	☐	☐
LAI of sub-canopy vascular	Uniform (Median value)	☐	☐	☐	☐	☐	☐	☐	☐	☐		
	Randomly assigned from measured distribution										☐	☐
Ground cover species	Uniform Bare peat				☐							
	Uniform *Cladonia. sp*			☐								
	Uniform *S. fuscum*		☐									
	Uniform *P. schreberi*	☐										
	Weighted based on % cover					☐	☐	☐				
	Spatially explicit (Mars)								☐	☐	☐	☐
Surface resistance (ground cover & sub-canopy vascular)	Uniform (Median value)	☐	☐	☐	☐	☐	☐	☐	☐	☐		
	Randomly assigned from measured distribution										☐	
	Temporal relationship											☐

TABLE 1 (Continued)

		SGBL-PS (*P. schreberi -big-leaf*)	SGBL-SF (*S. fuscum big-leaf*)	SGBL-C (*Cladonia sp. big-leaf*)	SGBL-BP (*bare peat big-leaf*)	WGBL (*weighted groundcover big-leaf*)	WGBL FFP (*weighted groundcover & mean canopy of footprint area*)	WGSC (*weighted groundcover & spatially explicit canopy*)	SGSC (*spatially distributed groundcover, & spatially explicit canopy*)	SGSCSM (*spatially distributed groundcover, micro-topography & canopy*)	SE (*everything is spatially explicit*)	STE (*everything is spatially explicit plus time relationship of r_s*)
	applied to value randomly assigned from measured distribution											
Micro-topography	Uniform (Median value)	□	□	□	□	□	□	□	□			
	Randomly assigned from measured distribution									□	□	□

3.2 | Impact of spatial complexity on simulated ET dynamics

Big-leaf (SGBL) models account for the smallest proportion of the variance observed in measured ET. Of these simulations SGBL-SF has the highest explained variance with an R^2 of 0.77 (Table 2). The scenario where the groundcover was weighted to represent the relative contributions of each cover type (WGBL) also had an R^2 of 0.77. Using mean radiation inputs from the footprint area at each time interval (WGBL-FFP) only improved R^2 to 0.79. A marked increase in explained variance (R^2 increased to 0.87) and reduction in root mean square error (RMSE) were observed when canopy and radiation were included in a spatially explicit manner within the simulation (Table 2). The increase in explained variance corresponded with a reduction in hysteresis amplitude between measured and simulated ET (reduction of the semi minor [width of ellipse] of 20%; Table 2, Figure 3, Figure SI-9 and Table SI-4) compare (a) to (f) with (g) to (j). Including temporally variable surface resistance of groundcover showed a slight reduction in unexplained variance of 0.04 with a corresponding hysteresis amplitude reduction (reduction of the of the semi minor [width of ellipse] of 41%; Table 2 and Figure 3), Figure SI-9 and Table SI-4, compare (j) and (k). No substantial changes in explained variance were observed when micro-topography, spatially distributed groundcover species, sub-canopy LAI and spatially variable surface resistances were included in model simulations (Table 2). Trees, sub-canopy vascular and groundcover relative contributions to ET vary among scenarios (Table 3). Tree transpiration was consistently the lowest contributor, ranging from 0.22% to 1.36% of total ET (Table 3). Groundcover contributions to ET dominated in all scenarios except SGBL-BP/C/PS, where sub-canopy vascular contributions show highest contributions to ET (Table 3; Figure 3). Figure 4 is presented to illustrate diurnal meteorological controls on ET. Figure 4 shows how the ratio of temperature to vapour pressure deficit changed throughout the day. Between the hours of 0900 and 1230, the ratio was ~1, indicating that both the surface atmosphere temperature gradient and vapour density deficit of the air (vdd_a) drove ET, whilst between the hours of 1300 and 0830, the ratio was <1, indicating that, vdd_a was the dominant driver of simulated ET.

4 | DISCUSSION

4.1 | How do the model scenarios and measured data estimates compare?

All simulations, except SGBL-PS and SGBL-C, overestimate ET (Table 2). In all scenarios where *S. fuscum* (the dominant groundcover type in the measured system) is represented, ET from the ground layer is the dominant ET contributor and supports wider research findings (Bisbee et al., 2001; Bond-Lamberty et al., 2011; Gabrielli, 2016; Heijmans et al., 2004a). Big-leaf model simulations with uniform groundcover of *Cladonia. sp*, *P. schreberi* and bare peat (SGBL – C/PS/BP) show lowest ET estimates and are considerably lower than a

TABLE 2 Descriptive statistics and Mann–Whitney U test results comparing gap filled measured eddy covariance flux data and data from each simulation (data shown in Figures 2 and 3).

	Scenario	Mean (mm d^{-1})	±SD (mm d^{-1})	*p*-value (<0.05)	% difference from measured	R^2	RMSE (mm d^{-1})
Gap-filled data	(a) SGBL-BP	2.54	2.63	<0.001	4.39	0.75	0.08
	(b) SGBL -C	2.20	2.25	<0.001	−10.68	0.74	0.08
	(c) SGBL-PS	2.34	2.41	<0.001	−3.76	0.75	0.08
	(d) SGBL -SF	3.56	3.78	<0.001	31.6	0.77	0.07
	(e) WGBL	3.15	3.33	<0.001	22.82	0.77	0.07
	(f) WGBL-FFP	3.47	3.76	<0.001	30.24	0.79	0.07
	(g) WGSC	4.38	4.87	<0.001	44.45	0.87	0.06
	(h) SGSC	4.51	5.05	<0.001	46.14	0.87	0.06
	(i) SGSCSM	4.55	5.09	<0.001	46.52	0.87	0.06
	(j) SE	3.81	4.32	<0.001	36.10	0.88	0.06
	(k) STE	3.89	4.46	<0.001	37.51	0.89	0.05
	EC ET	2.43	3.71	—	—	—	—

Note: (a) SGBL-BP (Bare Peat big-leaf), (b) SGBL-C (*Cladonia sp*. big-leaf), (c) SGBL-PS (*P. schreberi* -big-leaf), (d) SGBL-SF (*S. fuscum* big-leaf), (e) WGBL (Weighted groundcover big-leaf), (f) WGBL-FFP (Weighted groundcover & mean canopy of footprint area), (g) WGSC (Weighted groundcover & Spatially explicit canopy), (h) SGSC (Spatially distributed groundcover, & Spatially explicit canopy), (i) SGSCSM (Spatially distributed groundcover, micro- topography & canopy), (j) SE (Everything is spatially explicit), (k) STE (Everything is spatially explicit plus time relationship of rs).
Source: Data from boreal peatland system in summer.

TABLE 3 Relative contributions of each vertical system layer to ET (modelled data), for each scenario.

	Ground cover ET (%)	Tree ET (%)	Sub-canopy vascular ET (%)	Ground cover ET (mm d^{-1})	Tree ET (mm d^{-1})	Sub-canopy vascular (mm d^{-1})	Total mean (mm d^{-1})
SGBL-BP	44.49	1.18	54.33	1.13	0.03	1.38	2.54
SGBL-C	34.55	1.36	64.09	0.76	0.03	1.41	2.20
SGBL-PS	39.15	1.28	59.57	0.92	0.03	1.40	2.34
SGBL-SF	60.11	0.84	39.04	2.14	0.03	1.39	3.56
WGBL	59.37	0.95	39.68	1.87	0.03	1.25	3.15
WGBL-FFP	59.94	0.28	37.75	2.08	0.01	1.31	3.47
WGSC	54.69	0.23	45.08	2.39	0.01	1.97	4.38
SGSC	56.19	0.22	43.58	2.54	0.01	1.97	4.52
SGSCSM	56.48	0.22	43.30	2.57	0.01	1.97	4.55
SE	63.42	0.26	36.32	2.41	0.01	1.38	3.81
STE	62.17	0.34	37.5	2.35	0.01	1.42	3.89

Note: (a) SGBL-BP (Bare Peat big-leaf), (b) SGBL-C (*Cladonia sp*. big-leaf), (c) SGBL-PS (*P. schreberi* -big-leaf), (d) SGBL-SF (*S. fuscum* big-leaf), (e) WGBL (Weighted groundcover big-leaf), (f) WGBL-FFP (Weighted groundcover & mean canopy of footprint area), (g) WGSC (Weighted groundcover & Spatially explicit canopy), (h) SGSC (Spatially distributed groundcover, & Spatially explicit canopy), (i) SGSCSM (Spatially distributed groundcover, micro- topography & canopy), (j) SE (Everything is spatially explicit), (k) STE (Everything is spatially explicit plus time relationship of rs).

uniform cover of *S. fuscum* (SGBL-SF; Table 2) because of their significantly higher surface resistance (SI-1). The large difference between mean ET estimates within the four SGBL scenarios is because *Sphagnum* surface resistance (r_s) is significantly lower than other groundcover types (Heijmans et al., 2004a, 2004b; Leonard et al., 2018; Leonard et al., 2021), resulting in greater ground layer ET (Table 3). As a result, where the relative proportions of groundcovers and their respective surface resistance and albedo are represented (WGBL and WGBL-FFP), and where the low surface resistance *Sphagnum* only represents 43% cover, ET estimates are lower than SGBL-SF but still higher than SGBL-C/BP/PS. Increases in simulated ET occurs when mean radiation and canopy openness from the flux footprint at each time interval is applied, as opposed to the mean canopy and radiation inputs from 250 m radius of the tower. This is likely due to differences in radiation inputs between the mean radiation input for the 250 m radius and the mean for each time interval (based on footprint area).

The higher ET in simulations incorporating a spatially explicit canopy (WGSE, SGSC, SGSCSM and SE) likely results from the non-linear

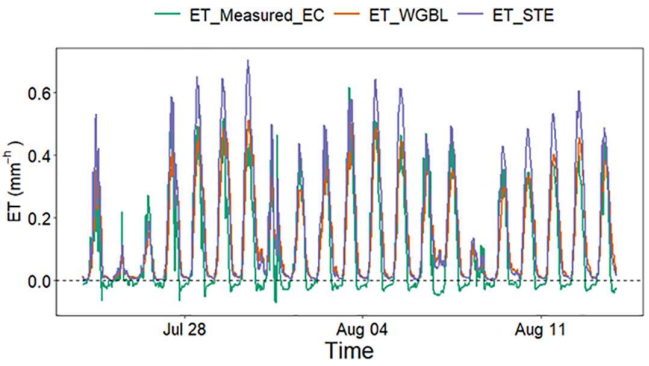

FIGURE 2 Time series of measured ET (gap-filled) from the EC tower, modelled ET from the detailed simulation (*k*) SE and ET modelled from simulation with 'big-leaf' canopy parameterization and weighted groundcover (*e*) WGBL.

response of groundcover ET to increased energy inputs. Spatial variability in the tree canopy and associated radiation inputs induce highly variable surface temperatures (Leonard et al., 2018; Leonard et al., 2021). Resultant high temperature patches of a given ground cover contribute dis-proportionately more to ET than the concurrent low energy lower temperature areas of the same ground cover type. This effect results from the non-linearity in the slope of the saturation humidity versus temperature curve (*s*) (Oke, 1987). Surfaces receiving the mean energy input evaporate less than the mean of surfaces receiving patches of higher and lower energy inputs. Tree transpiration was the lowest contributor to the overall ET budget in all simulations (0.22%–1.36%: Table 3), which is in agreement with literature estimates of 0.4%–34% (Thompson et al., 2014; Warren et al., 2018) and findings from other open-canopy systems (Allen, 1990; Baldocchi et al., 2000; Villegas et al., 2010, 2014; Vogel & Baldocchi, 1996; Yunusa et al., 1997). The very low contribution of transpiration to ET is largely due to the low sapwood area from short (2.3 m average height) and sparse (basal area of 11 m^2 ha^{-1}) black spruce canopy in northern peatlands (Angstmann et al., 2012; Mao et al., 2017; Wieder et al., 2009) in combination with saturated nutrient-poor soil and cold conditions adversely affecting transpiration (Bovard et al., 2005; Lieffers & Macdonald, 1989; Oren & Pataki, 2001; Simard et al., 2007). There is a slight decrease in transpiration rates when the scenario accounts for footprint area. The likely cause of this difference is variability in sapwood density mean values derived from 250 m radius area and the footprint area at each time interval.

The inclusion of spatially variable LAI and groundcover/sub-canopy surface resistance reduced ET overestimation. The log normal distribution in groundcover r_s creates areas of high surface resistance and low ground layer ET (Table 3). In addition, ET from the sub-canopy vascular layer in this simulation is reduced more substantially (Table 3). This is likely the combined effect of the log-normal distribution in sub-canopy LAI and stomatal resistance creating areas of low LAI and areas of high stomatal resistance that reduces the contribution of the vascular layer to system ET. Micro-topography and a distributed groundcover had relatively little impact on simulated ET (Figure 3, Table 2).

4.2 | Why does including complexity induce changes in system dynamics?

Including spatially explicit parameterisation of the canopy and radiation inputs has a noticeable impact on simulated ET (Table 2, Figure 3). Incorporation of small-scale spatio-temporal variability in canopy and radiation inputs reduced the magnitude of hysteresis in simulated ET (Figure 3, Figure SI-9 Table SI-4) because of the more detailed representation of the surface temperature component of the evaporation equation ($s[T_s - T_a]$), Equation (1). The reduction in the hysteresis amplitude (semi minor distance) results from increased simulated ET in the mornings (08:00 to 13:00), with negligible shift in ET through the subsequent afternoons (Figure 3). During the morning, between ~08:00 and ~13:00, the simulated ET is driven both by the surface atmosphere temperature gradient and vapour density deficit of the air (vdd_a; Figure 4). After ~13:00, vdd_a is the dominant driver of simulated ET (Figure 4). Spatial variation in surface temperature therefore has a minimal impact on ET during this time (Figure 3).

A likely reason for this overestimation of ET in the afternoon and remaining hysteresis in spatially (but not temporally) variable simulations (Figure 3g–j) is that the surface resistance values in the model do not change throughout the day (and are based on measurements between 10:00 and 16:00), whereas in the measured system (study site), ET values are probably increasing substantially in the afternoons (~16:00). Surface resistance is at around 100–300 s m^{-1} during the day, increasing towards the afternoon, and shows a strong increase from 15:00 to 18:00 of up to ~350% (Kellner, 2001). It is likely that surface evaporation demand exceeds supply in the afternoons, particularly when the water table is not near the surface. Different mosses/groundcover types have different capacities for meeting evaporative demand. *Sphagnum fuscum* can normally meet evaporative demands by wicking water up from depth using capillary rise (Hayward & Clymo, 1982; McCarter & Price, 2014; Price et al., 1997). However, other groundcover types, (including other *Sphagnum* spp., [McCarter & Price, 2014]), feather mosses (Carleton & Dunham, 2003) and lichens may dry out in afternoons due to their inability to access water from depth at a rate that meets evaporative demands. Overnight recharge processes that include fog, dew, distillation and capillary rise (Admiral & Lafleur, 2007; Carleton & Dunham, 2003; Yazaki et al., 2006) then function to reduce surface resistances at the start of the following day. The inclusion of diurnal trends in surface resistance values improves ET simulations and reduces the observed hysteresis by reducing afternoon ET (Figure 3k).

Once the temporal variability in surface resistance is included, hysteresis is reduced in the 0.2 to 0.4 mm d^{-1} range (Figure 3) and R^2 improves by 0.04–0.74. The remaining hysteresis is observed below 0.2 mm d^{-1}, when ET is lower, towards the start and end of the day (Figure 3). The hysteresis caused at the start and end of the day is likely a result of measurement and modelling uncertainty (although this does not appear to be a result of the energy balance closure correction applied to the measured data [compare Figure SI-7 with Figure SI-8]). There is uncertainty both in chamber (used to generate surface resistance values for groundcover types: SI-1) and EC measurements of ET. At the start and end of the day, chamber

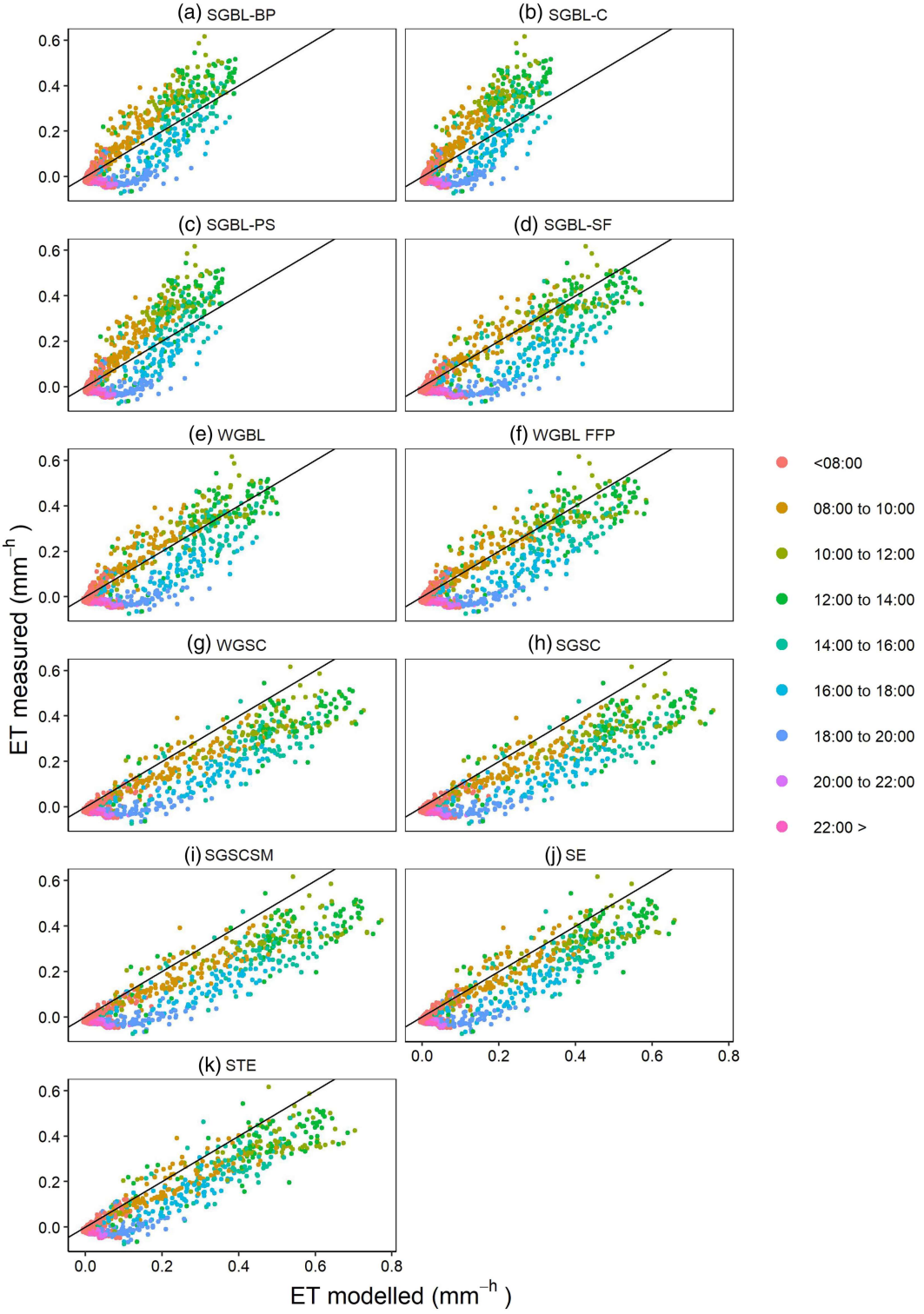

FIGURE 3 Correlation between 60-min eddy covariance ET data and ET modelled from corresponding footprint area for each simulation. 1:1 line shown on each tile (Gap-filled EC data included [60% gap-filled]). Colours show time of day.

measurements of the surface resistance are derived during periods of low ET and thus subject to high uncertainties (Kettridge et al., 2021) whilst EC measurements are predominantly gap-filled due to technical difficulties in flux measurement and subsequent processing. For example, friction velocity is more likely to fall below the threshold acceptance QA/QC threshold at these times because of reduced turbulence at night. Notably the non-gap filled data comparisons do not show hysteresis when temporally variable surface resistance is incorporated within model simulations (Figure SI-8). In addition, the BETA+ model unlikely represents the full complexity of the near-surface water and energy processes (condensation and evaporation) during the early hours of the day and within the early evening, as well as associated

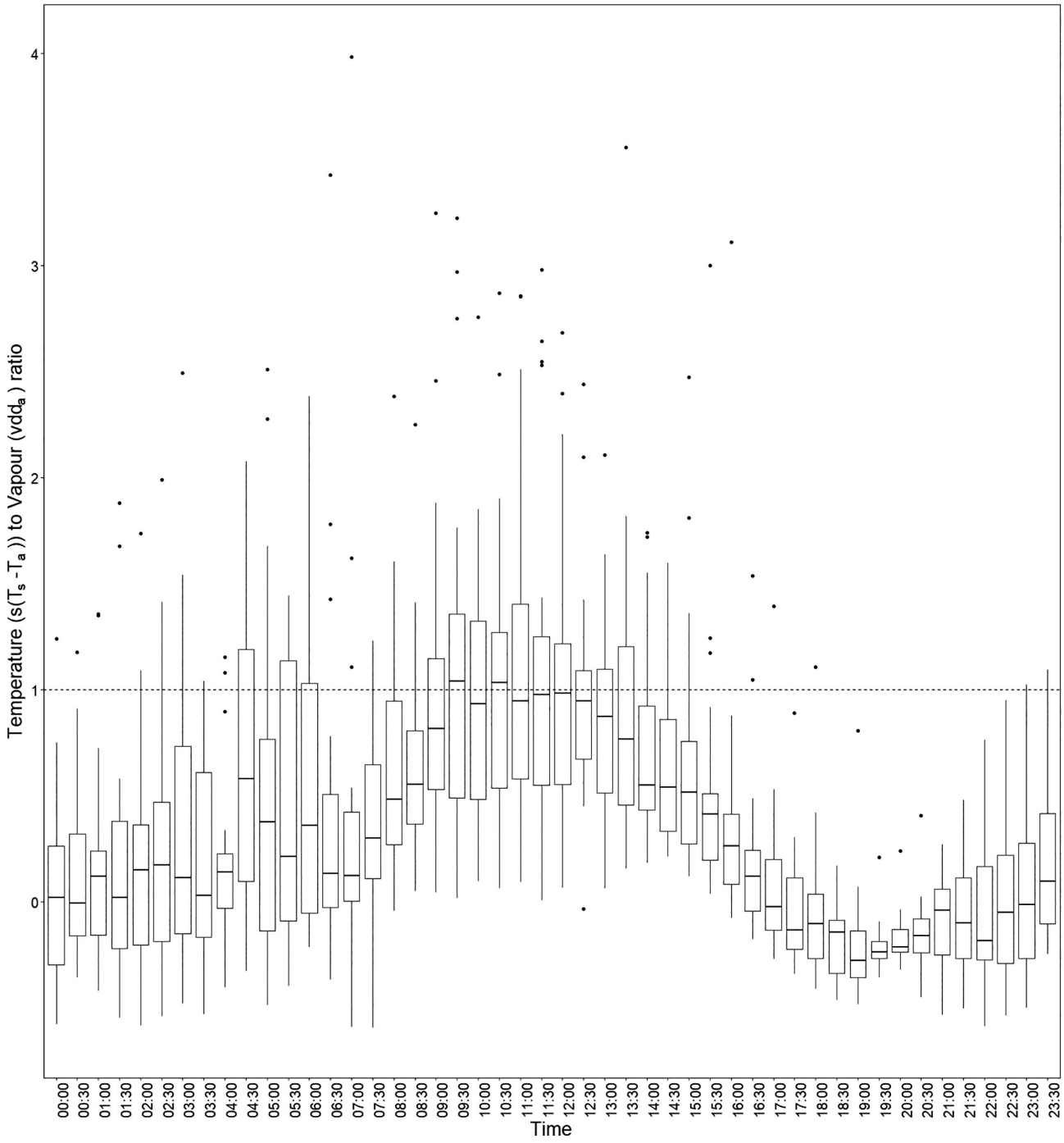

FIGURE 4 Boxplots of the ratio between the temperature (s [T_s–T_a]) and humidity (vdda) component of the evaporation equation (T_s is surface temperature, T_a is air temperature (K) and vdd_a is vapour density deficit of air (kg m^{-3}): Equation (1). Data are taken from entire simulation period and plotted at 30-min intervals between 0000 and 2330 from modelled data (STE). Boxplots represent the median, 25th and 75th percentile (whiskers: Smallest and largest observed value that's less than or equal to the lower/upper hinge ±1.5 * IQR)

surface resistances (evaporation and stomatal conductance) dynamics (Figure 2). However, the ET estimates at the start and end of the day have limited importance for overall ET estimates due to the lower rates of ET observed at this time. Simulations that incorporate micro-topography and the MARS sub-model predicting groundcover species distributions show relatively little changes in either mean ET, data variability (Figure 3, Table 2) or how the different layers contribute to overall ET (Table 3).

4.3 | Implications and further considerations for flux modelling

The magnitude of ET (EC data corrected for energy balance closure) was best replicated by the simpler model scenarios (SGBL-BP/C/PS, not SF). These scenarios however showed the greatest hysteresis (Figure 3, Figure SI-9 and Table SI-4) suggesting that key processes are not captured by the model. The results demonstrate that in open

canopy systems, spatial variability of energy inputs to below canopy are an important consideration for ET and can induce temporal changes in the landscape ET dynamics. Including spatio-temporal canopy and radiation variability in the model increases ET estimates by ~26% (gap filled data, 30.8% non-gap filled data) and reduces unexplained variance by 10% (when comparing gap filled big leaf simulation with weighted groundcover [WGBL-FFP] to spatially explicit canopy with weighted groundcover [WGSC]). Additionally, the inclusion of spatio-temporal canopy and radiation variability reduces hysteresis between measured and modelled data. Without this investigation into how complexity impacts ET and the data presented here, the observed hysteresis in big-leaf modelling results may have been explained solely as unaccounted for controls on ET, such as temporally dependent vegetation controls on surface resistance that vary diurnally, and in response to water availability (Betts et al., 2004; Kellner, 2001). Our results, however, suggest a substantial proportion of model variance may be explained by the spatio-temporal variability in energy inputs at the evaporating surface. This substantial decrease in unexplained variance is an important finding that quantifies the value added to predicting ET dynamics by incorporating the spatial variability of energy inputs. These results point out that even though the big-leaf model showed good estimations of ET, it is not representing some important mechanisms controlling and driving ET and in order to capture sub-daily ET temporal dynamics a spatially explicit model would be advantageous. The importance of this finding is highlighted further by the fact that the simulated system has a relatively uniform distribution of heterogeneity, that is, the tree canopy is variable in space but the distribution of the trees is relatively even (Figure 1). The observed effects of including a spatially explicit canopy and radiation representation would likely be stronger in a more heterogeneous system with even greater variability in energy inputs reaching the under-story (Kettridge et al., 2013).

5 | CONCLUSIONS

The evidence presented shows that accurate parameterisation of system structural layers that influence the spatio-temporal distribution of energy reaching the lower layers of forested ecosystems can provide more accurate ET dynamic predictions, especially for open canopy systems such as boreal forested peatlands. Results such as this have important implications for landscape scale modelling efforts and future climate predictions. Peatland ET can dominate landscape ET in regions such as the Boreal and improved representation of peatland controls on ET may in turn improve larger scale climate predictions (Helbig et al., 2020).

ACKNOWLEDGEMENTS

Thanks to Adam Green, George Sutherland, Patrick Pow, Max Lukenbach and Greg Carron for collection of eddy covariance data. We thank the Government of Alberta, Alberta Environment and Parks for the 2008 lidar data (under MoU 1907M20 a partnership with Dr Danielle Cobbaert, Dr Laura Chasmer and Dr Chris Hopkinson). We also thank Dr Thomas Pugh, Professor Fred Worrall, and two anonymous reviewers for their feedback on this work. Financial support was provided by a Natural Environment Research Council studentship funding (NE/L501712/1), Syncrude Canada Ltd. and Canadian Natural Resources Ltd. (SCL4600100599 to Kevin J. Devito, Richard M. Petrone, Carl Mendoza, Nicholas Kettridge and James Michael Waddington) and Natural Sciences and Engineering Research Council (NSERC-CRD, CRDPJ477235-14 to Kevin J. Devito, Richard M. Petrone, Carl Mendoza and James Michael Waddington).

DATA AVAILABILITY STATEMENT

The data that support the findings of this study are available from the corresponding author upon reasonable request.

ORCID

Rhoswen Leonard https://orcid.org/0000-0002-1358-0505
Paul Moore https://orcid.org/0000-0003-1924-1528
Stefan Krause https://orcid.org/0000-0003-2521-2248
Kevin J. Devito https://orcid.org/0000-0002-8216-0985
Richard M. Petrone https://orcid.org/0000-0002-9569-4337
Carl Mendoza https://orcid.org/0000-0002-2731-0004
Nicholas Kettridge https://orcid.org/0000-0003-3995-0305

REFERENCES

Aber, J. D., & Melillo, J. M. (2001). *Terrestrial Ecosystem* (2nd ed.). Academic Press.

Admiral, S. W., & Lafleur, P. M. (2007). Partitioning of latent heat flux at a northern peatland. *Aquatic Botany*, *86*(2), 107–116. https://doi.org/10.1016/j.aquabot.2006.09.006

Allen, S. J. (1990). Measurement and estimation of evaporation from soil under sparse barley crops in northern Syria. *Agricultural and Forest Meteorology*, *49*(4), 291–309. https://doi.org/10.1016/0168-1923(90)90003-O

Angstmann, J. L., Ewers, B. E., & Kwon, H. (2012). Size-mediated tree transpiration along soil drainage gradients in a boreal black spruce forest wildfire chronosequence. *Tree Physiology*, *32*(5), 599–611. https://doi.org/10.1093/treephys/tps021

Aubinet, M., Vesala, T., & Papale, D. (2012). *Eddy covariance: A practical guide to measurement and data analysis*. Springer & Business Media.

Baldocchi, D., Kelliher, F. M., Black, T. A., & Jarvis, P. (2000). Climate and vegetation controls on boreal zone energy exchange. *Global Change Biology*, *6*(S1), 69–83. https://doi.org/10.1046/j.1365-2486.2000.06014.x

Betts, A. K., Goulden, M. L., & Wofsy, S. C. (2004). Controls on evaporation in a black spruce forest. *Journal of Climate*, *12*, 1601–1618. https://doi.org/10.1029/2003GB002128

Bisbee, K., Gower, S., Norman, J., & Nordheim, E. (2001). Environmental controls on ground cover species composition and productivity in a boreal black spruce forest. *Oecologia*, *129*(2), 261–270. https://doi.org/10.1007/s004420100719

Black, T. A., Den Hartog, G., Neumann, H. H., Blanken, P. D., Yang, P. C., Russell, C., Nesic, Z., Lee, X., Chen, S. G., Staebler, R., & Novak, M. D. (1996). Annual cycles of water vapour and carbon dioxide fluxes in and above a boreal aspen forest. *Global Change Biology*, *2*(3), 219–229. https://doi.org/10.1111/j.1365-2486.1996.tb00074.x

Blanford, J. H., & Gay, L. W. (1992). Test of a robust eddy correlation system for sensible heat flux. *Theoretical and Applied Climatology*, *46*, 53–60. https://doi.org/10.1007/BF00866448

Boer, M. M., Bowman, D. M. J. S., Murphy, B. P., Cary, G. J., Cochrane, M. A., Fensham, R. J., Krawchuk, M. A., Price, O. F., De Dios, V. R., Williams, R. J., & Bradstock, R. A. (2016). Future changes in climatic water balance determine potential for transformational shifts

in Australian fire regimes. *Environmental Research Letters*, *11*(6), 65002. https://doi.org/10.1088/1748-9326/11/6/065002

Bonan, G. B. (2008). *Forests and climate*. Climate Benefits of Forests (June).

Bond-Lamberty, B., Gower, S. T., Amiro, B., & Ewers, B. E. (2011). Measurement and modelling of bryophyte evaporation in a boreal forest chronosequence. *Ecohydrology*, *4*, 26–35. https://doi.org/10.1002/eco.118

Bovard, B. D., Curtis, P. S., Vogel, C. S., Su, H. B., & Schmid, H. P. (2005). Environmental controls on sap flow in a northern hardwood forest. *Tree Physiology*, *25*(1), 31–38. https://doi.org/10.1093/treephys/25.1.31

Bradshaw, C. J. A., & Warkentin, I. G. (2015). Global estimates of boreal forest carbon stocks and flux. *Global and Planetary Change*, *128*, 24–30. Elsevier B.V. https://doi.org/10.1016/j.gloplacha.2015.02.004

Breshears, D. D., Whicker, J. J., Zou, C. B., Field, J. P., & Allen, C. D. (2009). A conceptual framework for dryland aeolian sediment transport along the grassland-forest continuum: Effects of woody plant canopy cover and disturbance. *Geomorphology*, *105*(1–2), 28–38. Elsevier B.V. https://doi.org/10.1016/j.geomorph.2007.12.018

Brown, M., & Lowe, D. G. (2005). Unsupervised 3D object recognition and reconstruction in unordered datasets. *Fifth International Conference on 3-D Digital Imaging and Modeling*, 56–63. https://doi.org/10.1109/3DIM.2005.81

Brümmer, C., Black, T. A., Jassal, R. S., Grant, N. J., Spittlehouse, D. L., Chen, B., Nesic, Z., Amiro, B. D., Arain, M. A., Barr, A. G., Bourque, C. P. A., Coursolle, C., Dunn, A. L., Flanagan, L. B., Humphreys, E. R., Lafleur, P. M., Margolis, H. A., McCaughey, J. H., & Wofsy, S. C. (2012). How climate and vegetation type influence evapotranspiration and water use efficiency in Canadian forest, peatland and grassland ecosystems. *Agricultural and Forest Meteorology*, *153*, 14–30. https://doi.org/10.1016/j.agrformet.2011.04.008

Brutsaert, W. (2010). *Evaporation into the atmosphere: Theory, history, and applications* (Vol. 1). Springer Science & Business Media. https://doi.org/10.1007/978-94-017-1497-6_1

Burba, G., Schmidt, A., Scott, R. L., Nakai, T., Kathilankal, J., Fratini, G., Hanson, C., Law, B., McDermitt, D. K., Eckles, R., & Furtaw, M. (2012). Calculating CO_2 and H_2O eddy covariance fluxes from an enclosed gas analyzer using an instantaneous mixing ratio. *Global Change Biology*, *18*(1), 385–399. https://doi.org/10.1111/j.1365-2486.2011.02536.x

Burgess, S. S. O., Adams, M. A., Turner, N. C., Beverly, C. R., Ong, C. K., Khan, A. A. H., & Bleby, T. I. M. M. (2001). An improved heat pulse method to measure low and reverse rates of sap flow in woody plants. *Tree Physiology*, *21*(1998), 589–598.

Burton, P. J. (2013). Exploring complexity in boreal forests. In M. Christian, K. J. Puettmann, & D. Coates (Eds.), *Managing forests as complex adaptive systems: Building resilience to the challenge of global change* (pp. 79–110). Routledge. https://doi.org/10.4324/9780203122808

Carleton, T. J., & Dunham, K. M. M. (2003). Distillation in a boreal mossy forest floor. *Canadian Journal of Forest Research*, *33*(4), 663–671. https://doi.org/10.1139/x02-197

Chapin, F. S., Mcguire, A. D., Randerson, J., Pielke, R., Baldocchi, D., Hobbie, S. E., Roulet, N., Eugster, W., Kasischke, E., Rastetter, E. B., & Zimov, S. A. (2000). Arctic and boreal ecosystems of western North America as components of the climate system. *Global Change Biology*, *6*, 211–223. https://doi.org/10.1046/j.1365-2486.2000.06022.x

Ciais, P., Sabine, C., Bala, G., Bopp, L., Brovkin, V., Canadell, J., Chhabra, A., DeFries, R., Galloway, J., Heimann, M., & Jones, C. (2013). Carbon and other biogeochemical cycles. In V. B, P. M. M. Stocker, T. F, D. Qin, G.-K. Plattner, M. Tignor, S. K. Allen, J. Boschung, A. Nauels, & Y. Xia (Eds.), *Climate change 2013: The physical science basis. Working group I contribution to the 5th assessment of the intergovernmental panel on climate change*. Cambridge University Press.

Davis, T. W., Kuo, C.-M., Liang, X., & Yu, P.-S. (2012). Sap flow sensors: Construction, quality control and comparison. *Sensors*, *12*(12), 954–971. https://doi.org/10.3390/s120100954

Devito, K., Creed, I., Gan, T., Mendoza, C., Petrone, R., Silins, U., & Smerdon, B. (2005). A framework for broad-scale classification of hydrologic response units on the boreal plain: Is topography the last thing to consider? *Hydrological Processes*, *19*(8), 1705–1714. https://doi.org/10.1002/hyp.5881

Devito, K. J., Hokanson, K. J., Moore, P. A., Kettridge, N., Anderson, A. E., Chasmer, L., Hopkinson, C., Lukenbach, M. C., Mendoza, C. A., Morissette, J., Peters, D. L., Petrone, R. M., Silins, U., Smerdon, B., & Waddington, J. M. (2017). Landscape controls on long-term runoff in subhumid heterogeneous Boreal Plains catchments. *Hydrological Processes*, *31*(15), 2737–2751. https://doi.org/10.1002/hyp.11213

Devito, K. J., Mendoza, C., Petrone, R. M., Kettridge, N., & Waddington, J. M. (2016). Utikuma region study area (URSA)—Part 1: Hydrogeological and ecohydrological studies (HEAD). *The Forestry Chronicle*, *92*(1), 57–61.

Elith, J., & Leathwick, J. (2007). Predicting species distributions from museum and herbarium records using multiresponse models fitted with multivariate adaptive regression splines. *Diversity and Distributions*, *13*(3), 265–275. https://doi.org/10.1111/j.1472-4642.2007.00340.x

Ellison, D., Morris, C. E., Locatelli, B., Sheil, D., Cohen, J., Murdiyarso, D., Gutierrez, V., Van Noordwijk, M., Creed, I. F., Pokorny, J., & Gaveau, D. (2017). Trees, forests and water: Cool insights for a hot world. *Global Environmental Change*, *43*, 51–61. Elsevier Ltd. https://doi.org/10.1016/j.gloenvcha.2017.01.002

Essery, R., Bunting, P., Rowlands, A., Rutter, N., Hardy, J., Melloh, R., Link, T., Marks, D., & Pomeroy, J. (2008). Radiative transfer modeling of a coniferous canopy characterized by airborne remote sensing. *Journal of Hydrometeorology*, *9*(2), 228–241. https://doi.org/10.1175/2007JHM870.1

Farouki, O. (1986). *Thermal properties of soils, series on rock and soil mechanics* (Vol. 11). Trans Tech Publications.

Fatichi, S., & Pappas, C. (2017). Constrained variability of modeled T:ET ratio across biomes. *Geophysical Research Letters*, *44*(13), 6795–6803. https://doi.org/10.1002/2017GL074041

Ferretti, D. F., Pendall, E., Morgan, J. A., Nelson, J. A., LeCain, D., & Mosier, A. R. (2003). Partitioning evapotranspiration fluxes from a Colorado grassland using stable isotopes: Seasonal variations and ecosystem implications of elevated atmospheric CO2. *Plant and Soil*, *254*(2), 291–303. https://doi.org/10.1023/A:1025511618571

Foken, T., & Leclerc, M. Y. (2004). Methods and limitations in validation of footprint models. *Agriculture and Forest Meteorology*, *127*(3–4), 223–234.

Friend, A. D. (2001). Modelling canopy CO2 fluxes: Are 'big-leaf' simplifications justified? *Global Ecology and Biogeography*, *10*(6), 603–619. https://doi.org/10.1046/j.1466-822x.2001.00268.x

Gabrielli, E. C. (2016). *Partitioning evapotranspiration in forested peatlands within the western boreal plain, Fort McMurray, Alberta, Canada* [Theses and Dissertations (Comprehensive)]. 1820. https://scholars.wlu.ca/etd/1820

Green, F. H. W., Harding, R. J., & Oliver, H. R. (1984). The relationship of soil temperature to vegetation height. *Journal of Climatology*, *4*(3), 229–240. https://doi.org/10.1002/joc.3370040302

Hayward, P. M., & Clymo, R. S. (1982). Profiles of water content and pore size in sphagnum and peat, and their relation to peat bog ecology. *Proceedings of the Royal Society B: Biological Sciences*, *215*, 299–325. https://doi.org/10.1098/rspb.1982.0044

Heijmans, M. M. P. D., Arp, W. J., & Chapin, F. S. (2004a). Carbon dioxide and water vapour exchange from understory species in boreal forest. *Agricultural and Forest Meteorology*, *123*, 135–147. https://doi.org/10.1016/j.agrformet.2003.12.006

Heijmans, M. M. P. D., Arp, W. J., & Chapin, F. S. (2004b). Controls on moss evaporation in a boreal black spruce forest. *Global Biogeochemical Cycles*, *18*(2), n/a-n/a. https://doi.org/10.1029/2003GB002128

Helbig, M., Waddington, J., Alekseychik, P., Amiro, B., Aurela, M., Barr, A., Black, T., Blanken, P. D., Carey, S. K., Chen, J., & Chi, J. (2020).

Increasing contribution of peatlands to boreal evapotranspiration in a warming climate. *Nature Climate Change*, *10*, 1–6. https://doi.org/10.1038/s41558-020-0763-7

Holden, J. (2005). Peatland hydrology and carbon release: Why small-scale process matters. *Philosophical Transactions of the Royal Society A - Mathematical Physical and Engineering Sciences*, *363*(1837), 2891–2913. https://doi.org/10.1098/rsta.2005.1671

Hossein, A. O., P., W., & T., P. U. K. (1994). Partitioning of evapotranspiration using lysimeter and micro-bowen-ratio system. *Journal of Irrigation and Drainage Engineering*, *120*(2), 450–464. American Society of Civil Engineers. https://doi.org/10.1061/(ASCE)0733-9437(1994)120:2(450)

Jackson, R. B., Carpenter, S. R., Dahm, C. N., McKnight, D. M., Naiman, R. J., Postel, S. L., & Running, S. W. (2001). Water in a changing world. *Ecological Applications*, *11*(4), 1027–1045. https://doi.org/10.1890/1051-0761(2001)011[1027:WIACW]2.0.CO;2

Joos, F., Roth, R., Fuglestvedt, J. S., Peters, G. P., Enting, I. G., Von Bloh, W., Brovkin, V., Burke, E. J., Eby, M., Edwards, N. R., & Friedrich, T. (2013). Carbon dioxide and climate impulse response functions for the computation of greenhouse gas metrics: A multi-model analysis. *Atmospheric Chemistry and Physics*, *13*(5), 2793–2825. https://doi.org/10.5194/acp-13-2793-2013

Joosten, H., & Clarke, D. (2002). *Wise use of mires and peatlands - Background and principles including framework for decision - making*. International Mire Conservation Group andInternational Peat Society.

Kaimal, J. C., & Finningan, J. (1994). *Atmospheric Bournary layer flows: Their structure and measurement*. Oxford University Press.

Kellner, E. (2001). Surface energy fluxes and control of evapotranspiratoin from a Swedish sphagnum mire. *Agricultural and Forest Meteorology*, *110*(2), 101–123. https://doi.org/10.1016/S0168-1923(01)00283-0

Kettridge, N., & Baird, A. J. (2010). Simulating the thermal behavior of northern peatlands with a 3-D microtopography. *Journal of Geophysical Research*, *115*(G3), G03009. https://doi.org/10.1029/2009JG001068

Kettridge, N., Lukenbach, M. C., Hokanson, K. J., Devito, K. J., Petrone, R. M., Mendoza, C. A., & Waddington, J. M. (2021). Regulation of peatland evaporation following wildfire; the complex control of soil tension under dynamic evaporation demand. *Hydrological Processes*, *35*(4), e14132. https://doi.org/10.1002/hyp.14132

Kettridge, N., Thompson, D. K., Bombonato, L., Turetsky, M. R., Benscoter, B. W., & Waddington, J. M. (2013). The ecohydrology of forested peatlands: Simulating the effects of tree shading on moss evaporation and species composition. *Journal of Geophysical Research – Biogeosciences*, *118*(2), 422–435. https://doi.org/10.1002/jgrg.20043

Kettridge, N., Thompson, D. K., & Waddington, J. M. (2012). Impact of wildfire on the thermal behavior of northern peatlands: Observations and model simulations. *Journal of Geophysical Research – Biogeosciences*, *117*(G2), n/a-n/a. https://doi.org/10.1029/2011JG001910

Kljun, N., Calanca, P., Rotach, M. W., & Schmid, H. P. (2015). A simple two-dimensional parameterisation for flux footprint prediction (FFP). *Geoscientific Model Development*, *8*(11), 3695–3713. https://doi.org/10.5194/gmd-8-3695-2015

Kurz, W. A., & Apps, M. J. (1993). In J. Wisniewski & R. N. Sampson (Eds.), *Contribution of northern forests to the global C cycle: Canada as a case study BT - terrestrial Biospheric carbon fluxes quantification of sinks and sources of CO2* (pp. 163–176). Springer Netherlands. https://doi.org/10.1007/978-94-011-1982-5_10

Lafleur, P. (1990). Evaporation from wetlands. *The Canadian Geographer / Le Géographe canadien*, *34*(1), 79–82. https://doi.org/10.1111/j.1541-0064.1990.tb01072.x

Landsberg, J. J., & Gower, S. T. (1997). *Applications of physiological ecology to forest management*. Academic Press Retrieved from http://lib.ugent.be/catalog/rug01:000478902

Leonard, R., Moore, P., Krause, S., Devito, K. J., Petrone, G. R., Mendoza, C., Waddington, J. M., & Kettridge, N. (2021). The influence of system heterogeneity on peat-surface temperature dynamics. *Environmental Research Letters*, *16*(2), 024002. https://doi.org/10.1088/1748-9326/abd4ff

Leonard, R. M., Kettridge, N., Devito, K. J., Petrone, R. M., Mendoza, C. A., Waddington, J. M., & Krause, S. (2018). Disturbance impacts on thermal hot spots and hot moments at the peatland-atmosphere Interface. *Geophysical Research Letters*, *1–9*, 185–193. https://doi.org/10.1002/2017GL075974

Leuning, R., Condon, A. G., Dunin, F. X., Zegelin, S., & Denmead, O. T. (1994). Rainfall interception and evaporation from soil below a wheat canopy. *Agricultural and Forest Meteorology*, *67*(3–4), 221–238. https://doi.org/10.1016/0168-1923(94)90004-3

Leuning, R., & Judd, M. J. (1996). The relative merits of open- and closed-path analysers for measurement of eddy fluxes. *Global Change Biology*, *2*(3), 241–253. https://doi.org/10.1111/j.1365-2486.1996.tb00076.x

Lieffers, V. J., & Macdonald, S. E. (1989). Growth and foliar nutrient status of black spruce and tamarack in relation to depth of water table in some Alberta peatlands. *Canadian Journal of Forest Research*, *20*(6), 805–809. https://doi.org/10.1139/x90-106

Mao, L., Bater, C. W., Stadt, J. J., White, B., Tompalski, P., Coops, N. C., & Nielsen, S. E. (2017). Environmental landscape determinants of maximum forest canopy height of boreal forests. *Journal of Plant Ecology*, *12*(1), 96–102. https://doi.org/10.1093/jpe/rtx071

Martens, S. N., Breshears, D. D., & Meyer, C. W. (2000). Spatial distributions of understory light along the grassland/forest continuum: Effects of cover, height, and spatial pattern of tree canopies. *Ecological Modelling*, *126*(1), 79–93. https://doi.org/10.1016/S0304-3800(99)00188-X

Mccarter, C. P. R., & Price, J. S. (2014). Ecohydrology of sphagnum moss hummocks: Mechanisms of capitula water supply and simulated effects of evaporation. *Ecohydrology*, *7*(1), 33–44. https://doi.org/10.1002/eco.1313

McCarthy, J. (2001). Gap dynamics of forest trees: A review with particular attention to boreal forests. *Environmental Reviews*, *9*(2), 129. https://doi.org/10.1139/er-9-2-129

McGuire, D. A., Melillo, J. M., Kicklighter, D. W., & Joyce, L. A. (1995). Equilibrium responses of soil carbon to climate change: Empirical and process-based estimates. *Journal of Biogeography*, *22*(4/5), 785–796 Retrieved from http://www.jstor.org/stable/2845980

McKenzie, J. M., Voss, C. I., & Siegel, D. I. (2007). Groundwater flow with energy transport and water–ice phase change: Numerical simulations, benchmarks, and application to freezing in peat bogs. *Advances in Water Resources*, *30*(4), 966–983. https://doi.org/10.1016/j.advwatres.2006.08.008

McNaughton, K. G., & Jarvis, P. G. (1983). Predicting effects of vegetation changes on transpiration and evaporation. In T. Kozlowski (Ed.), *Water deficits and plant growth* (pp. 1–47). Acadmic Press.

Moore, P. A., Lukenbach, M. C., Thompson, D. K., Kettridge, N., Granath, G., & Waddington, J. M. (2019). Assessing the peatland hummock-hollow classification framework using high-resolution elevation models: Implications for appropriate complexity ecosystem modeling. *Biogeosciences*, *16*(18), 3491–3506. https://doi.org/10.5194/bg-16-3491-2019

Nungesser, M. K. (2003). Modelling microtopography in boreal peatlands: Hummocks and hollows. *Ecological Modelling*, *165*(2–3), 175–207. https://doi.org/10.1016/S0304-3800(03)00067-X

Oke, T. R. (1987). *Boundary layer climates* (2nd ed.). Routledge.

Oren, R., & Pataki, D. E. (2001). Transpiration in response to variation in microclimate and soil moisture in southeastern deciduous forests. *Oecologia*, *127*(4), 549–559. https://doi.org/10.1007/s004420000622

Oren, R., Zimmermann, R., & Terbough, J. (1996). Transpiration in upper Amazonia floodplain and upland forests in response to drought- breaking rains. *Ecology*, *77*(3), 968–973 Retrieved from https://www.jstor.org/stable/2265517

Prather, M. J., Holmes, C. D., & Hsu, J. (2012). Reactive greenhouse gas scenarios: Systematic exploration of uncertainties and the role of atmospheric chemistry. *Geophysical Research Letters*, *39*(9), L09803. https://doi.org/10.1029/2012GL051440

Prentice, I. C., & Harrison, S. P. (2009). Ecosystem effects of CO2 concentration: Evidence from past climates. *Climate of the Past*, *5*(3), 297–307. https://doi.org/10.5194/cp-5-297-2009

Price, A., Dunham, K., Carleton, T., & Band, L. (1997). Variability of water fluxes through the black spruce (Picea mariana) canopy and feather moss (*Pleurozium schreberi*) carpet in the boreal forest of northern Manitoba. *Journal of Hydrology*, *196*(1–4), 310–323. https://doi.org/10.1016/S0022-1694(96)03233-7

Priestley, C. H., & Taylor, R. J. (1972). On the assessment of surface heat flux and evaporation using large-scale parameters. *Monthly Weather Review*, *100*(2), 81–92.

Sagar, R., Singh, A., & Singh, J. S. (2008). Differential effect of woody plant canopies on species composition and diversity of ground vegetation: A case study. *Tropical Ecology*, *49*(2), 189–197.

Schuepp, P. H., Leclerc, M. Y., Macpherson, J. I., & Desjardins, R. L. (1990). Footprint Predic- tion of scalar fluxes from analytical solutions of the diffusion equation. *Boundary-Layer Meteorology*, *50*, 353–373.

Sena, J., De, O. A., Zaidan, H. A., Castro, C. e., & De, P. R. (2007). Transpiration and stomatal resistance variations of perennial tropical crops under soil water availability conditions and water deficit. *Brazilian Archives of Biology and Technology*, *50*(2), 225–230.

Shuttleworth, W. J. (2007). Putting the 'vap' into evaporation. *Hydrology and Earth System Sciences*, *11*(1), 210–244. https://doi.org/10.5194/hess-11-210-2007

Simard, M., Lecomte, N., Bergeron, Y., Bernier, P. Y., & Paré, D. (2007). Forest productivity decline caused by successional paludification of boreal soils. *Ecological Applications*, *17*(6), 1619–1637. John Wiley & Sons, Ltd. https://doi.org/10.1890/06-1795.1 17, 1619, 1637.

Sutherland, G., Chasmer, L. E., Petrone, R. M., Kljun, N., & Devito, K. J. (2014). Evaluating the use of spatially varying versus bulk average 3D vegetation structural inputs to modelled evapotranspiration within heterogeneous land cover types. *Ecohydrology*, *7*(6), 1545–1559. https://doi.org/10.1002/eco.1477

Sutherland, G., Chasmer, L. E., Kljun, N., Devito, K. J., & Petrone, R. M. (2017). Using high resolution LiDAR data and a flux footprint parameterization to scale evapotranspiration estimates to lower pixel resolutions. *Canadian Journal of Remote Sensing*, *43*(2), 215–229. https://doi.org/10.1080/07038992.2017.1291338

Thompson, D. K., Benscoter, B. W., & Waddington, J. M. (2014). Water balance of a burned and unburned forested boreal peatland. *Hydrological Processes*, *28*(24), 5954–5964. https://doi.org/10.1002/hyp.10074

Turetsky, M., Wieder, K., Halsey, L., & Vitt, D. (2002). Current disturbance and the diminishing peatland carbon sink. *Geophysical Research Letters*, *29*(11), 7–10. https://doi.org/10.1029/2001GL014000

Villegas, J. C., Breshears, D. D., Zou, C. B., & Law, D. J. (2010). Ecohydrological controls of soil evaporation in deciduous drylands: How the hierarchical effects of litter, patch and vegetation mosaic cover interact with phenology and season. *Journal of Arid Environments*, *74*(5), 595–602. Elsevier Ltd. https://doi.org/10.1016/j.jaridenv.2009.09.028

Villegas, J. C., Espeleta, J. E., Morrison, C. T., Breshears, D. D., & Huxman, T. E. (2014). Factoring in canopy cover heterogeneity on evapotranspiration partitioning: Beyond big-leaf surface homogeneity assumptions. *Journal of Soil and Water Conservation*, *69*(3), 78A–83A. https://doi.org/10.2489/jswc.69.3.78a

Vogel, C. A., & Baldocchi, D. D. (1996). Energy and CO2 flux densities above and below a temperate broad-leaved forest and a boreal pine forest. *Tree Physiology*, *16*, 5–16.

Wallace, J. S., Lloyd, C. R., & Sivakumar, M. V. K. (1993). Measurements of soil, plant and total evaporation from millet in Niger. *Agricultural and Forest Meteorology*, *63*(3–4), 149–169. https://doi.org/10.1016/0168-1923(93)90058-P

Warren, R. K., Pappas, C., Helbig, M., Chasmer, L. E., Berg, A. A., Baltzer, J. L., Quinton, W. L., & Sonnentag, O. (2018). Minor contribution of overstorey transpiration to landscape evapotranspiration in boreal permafrost peatlands. *Ecohydrology*, *11*(5), 1–10. https://doi.org/10.1002/eco.1975

Watras, C. J. (2017). Estimates of evapotranspiration from contrasting Wisconsin peatlands based on diel water table oscillations (august 2016). *Ecohydrology*, *10*(4), e1834. https://doi.org/10.1002/eco.1834

Webb, E. K., Pearman, G. I., & Leuning, R. (1980). Correction of flux measurements for density effects. *Quarterly Journal of the Royal Meteorological Society*, *106*, 85–100.

Wieder, R. K., Scott, K. D., Kamminga, K., Vile, M. A., Vitt, D. H., Bone, T., Xu, B., Benscoter, B. W., & Bhatti, J. S. (2009). Postfire carbon balance in boreal bogs of Alberta, Canada. *Global Change Biology*, *15*(1), 63–81. https://doi.org/10.1111/j.1365-2486.2008.01756.x

Williams, D. G., Cable, W., Hultine, K., Hoedjes, J. C. B., Yepez, E. A., Simonneaux, V., Er-Raki, S., Boulet, G., de Bruin, H. A. R., Chehbouni, A., Hartogensis, O. K., & Timouk, F. (2004). Evapotranspiration components determined by stable isotope, sap flow and eddy covariance techniques. *Agricultural and Forest Meteorology*, *125*(3–4), 241–258. https://doi.org/10.1016/j.agrformet.2004.04.008

Wilson, K. (2002). Energy balance closure at FLUXNET sites. *Agricultural and Forest Meteorology*, *113*(1–4), 223–243. https://doi.org/10.1016/S0168-1923(02)00109-0

Wilson, K. B., Hanson, P. J., Mulholland, P. J., Baldocchi, D. D., & Wullschleger, S. D. (2001). A comparison of methods for determining forest evapotranspiration and its components: Sap-flow, soil water budget, eddy covariance and catchment water balance. *Agricultural and Forest Meteorology*, *106*(2), 153–168. https://doi.org/10.1016/S0168-1923(00)00199-4

Yazaki, T., Urano, S. I., & Yabe, K. (2006). Water balance and water movement in unsaturated zones of sphagnum hummocks in Fuhrengawa mire, Hokkaido, Japan. *Journal of Hydrology*, *319*(1–4), 312–327. https://doi.org/10.1016/j.jhydrol.2005.06.037

Yu, Z. C. (2012). Northern peatland carbon stocks and dynamics: A review. *Biogeosciences*, *9*(10), 4071–4085. https://doi.org/10.5194/bg-9-4071-2012

Yunusa, I. A. M., Walker, R. R., & Guy, J. R. (1997). Partitioning of seasonal evapotranspiration from a commercial furrow-irrigated sultana vineyard. *Irrigation Science*, *18*(1), 45–54. https://doi.org/10.1007/s002710050043

Zhang, K., Kimball, J. S., Mu, Q., Jones, L. A., Goetz, S. J., & Running, S. W. (2009). Satellite based analysis of northern ET trends and associated changes in the regional water balance from 1983 to 2005. *Journal of Hydrology*, *379*(1–2), 92–110. https://doi.org/10.1016/j.jhydrol.2009.09.047

Zhao, L., Xia, J., Xu, C. y., Wang, Z., Sobkowiak, L., & Long, C. (2013). Evapotranspiration estimation methods in hydrological models. *Journal of Geographical Sciences*, *23*(2), 359–369. https://doi.org/10.1007/s11442-013-1015-9

SUPPORTING INFORMATION

Additional supporting information can be found online in the Supporting Information section at the end of this article.

How to cite this article: Leonard, R., Moore, P., Krause, S., Chasmer, L., Devito, K. J., Petrone, R. M., Mendoza, C., Waddington, J. M., & Kettridge, N. (2022). Forest stand complexity controls ecosystem-scale evapotranspiration dynamics: Implications for landscape flux simulations. *Hydrological Processes*, *36*(12), e14761. https://doi.org/10.1002/hyp.14761